JVI03212-15 Version 2

Analyses of Coronavirus Assembly Interactions with Interspecies Membrane and Nucleocapsid Protein Chimeras

Lili Kuo, Kelley R. Hurst-Hess, Cheri A. Koetzner, and Paul S. Masters[#]

Wadsworth Center, New York State Department of Health, Albany, New York 12201

[#]Corresponding author. Mailing address: Griffin Laboratory, Wadsworth Center, NYSDOH, Empire State Plaza, P.O. Box 509, Albany, New York 12201-0509. Phone: (518) 485-6554. Fax: (518) 869-6487. E-mail: Paul.Masters@health.ny.gov.

Running title:

CORONAVIRUS M AND N PROTEIN ASSEMBLY INTERACTIONS

Abstract: 241 words

Text: 6527 words (excluding references and figure legends)

ABSTRACT

The coronavirus membrane (M) protein is the central actor in virion morphogenesis. M organizes the components of the viral membrane, and interactions of M with itself and with the nucleocapsid (N) protein drive virus assembly and budding. In order to further define M-M and M-N interactions we constructed mutants of the model coronavirus mouse hepatitis virus (MHV) in which all or part of the M protein was replaced by its phylogenetically divergent counterpart from severe acute respiratory syndrome coronavirus (SARS-CoV). We were able to obtain viable chimeras containing the entire SARS-CoV M protein as well as mutants with intramolecular substitutions that partitioned M protein at the boundaries between the ectodomain, transmembrane domains, or endodomain. Our results show that the carboxy-terminal domain of N protein, N3, is necessary and sufficient for interaction with M protein. However, despite some previous genetic and biochemical evidence that mapped interactions with N to the carboxy terminus of M, it was not possible to define a short linear region of M protein sufficient for assembly with N. Thus, interactions with N protein likely involve multiple linearly discontiguous regions of the M endodomain. The SARS-CoV M chimera exhibited a conditional growth defect that was partially suppressed by mutations in the envelope (E) protein. Moreover, virions of the M chimera were markedly deficient in spike (S) protein incorporation. These finding suggest that the interactions of M protein with both E and S protein are more complex than previously thought.

IMPORTANCE

The assembly of coronavirus virions entails concerted interactions among the viral structural proteins and the RNA genome. One strategy to study this process is through construction of interspecies chimeras that preserve or disrupt particular inter- or intramolecular associations. In this work, we replaced the membrane (M) protein of the model coronavirus mouse hepatitis virus with its counterpart from a heterologous coronavirus. The results clarify our understanding of the interaction between the coronavirus M protein and the nucleocapsid protein. At the same time they reveal unanticipated complexities in the interactions of M with the viral spike and envelope proteins.

INTRODUCTION

Coronaviruses are a family of enveloped positive-strand RNA viruses that cause disease in numerous mammalian and avian hosts (1, 2). Of the six coronaviruses that can infect humans, the two of greatest current concern are the etiologic agents of severe acute respiratory syndrome (SARS-CoV) and Middle East respiratory syndrome (MERS-CoV). Virions of coronaviruses contain a canonical set of four structural proteins. The most numerous constituent, the membrane (M) protein, makes up a lattice in the viral envelope that associates with the other components. Trimers of spike (S) protein form projections on the virion surface responsible for attachment to host cell receptors, and minor amounts of the small envelope (E) protein also appear in the viral membrane. In the virion interior, the nucleocapsid (N) protein encloses the ~30-kb viral genome into a helically symmetric ribonucleoprotein.

Much of our knowledge of coronavirus assembly has been worked out through studies with

68 the prototype mouse hepatitis virus (MHV). MHV falls into the betacoronaviruses, the second of the
69 four genera of the family and the one which also includes SARS-CoV and MERS-CoV. Key
70 contributions to understanding virion morphogenesis have also been made through analyses of the
71 gammacoronavirus infectious bronchitis virus (IBV) and the alphacoronavirus transmissible
72 gastroenteritis virus (TGEV). A large body of work points to M protein as the major player in virion
73 assembly. Coexpression of subsets of viral proteins revealed that just M protein and E protein are
74 sufficient for the formation of virus-like particles (VLPs) (3-5). The inclusion of N protein, although
75 it is not strictly required, greatly enhances the efficiency of VLP formation (6, 7). The critical role of
76 E protein is carried out at the site of budding, the endoplasmic reticulum-Golgi intermediate
77 compartment, with very little E being carried over into assembled virions (8). Additionally, M
78 protein captures S protein for incorporation into virions or VLPs (9, 10), but S is an optional
79 participant in virus formation (11, 12), even though it is essential for infectivity.

80 Thus, extensive networks of protein-protein interactions in coronavirus assembly involve one
81 or both of the most abundant virion components, M and N. The N protein is a highly basic
82 phosphoprotein containing structurally distinct amino-terminal and carboxy-terminal RNA-binding
83 domains (NTD and CTD) (13), which we have previously called domains N1b and N2b, respectively
84 (14-16) (Fig. 1A). In MHV N protein the CTD, but not the NTD, is a critical determinant for
85 recognition of the genomic RNA packaging signal (16). The CTD also mediates N-N dimerization
86 and longer-range interactions in the nucleocapsid (17). Flanking the NTD and CTD are intrinsically
87 disordered protein segments (13, 18). One of these, the linker between the NTD and CTD, harbors a
88 serine- and arginine-rich region that binds to the replicase nonstructural protein 3 in an interaction
89 crucial to an early step of infection (15, 19). At the carboxy terminus of the molecule is domain N3,
90 which many (20-24) but not all (25-27) prior studies have assigned as the locus of N-M interactions.

91 The M protein is a triple-spanning transmembrane protein with a small ectodomain and a

large carboxy-terminal endodomain (28, 29) (Fig. 1A). As yet, there is only limited structural information available for M. The assignment of intra- and intermolecular interactions to parts of the M protein is more tentative than for the N protein. Evidence from cryo-electron micrographic (EM) and tomographic reconstructions (30) and inferences drawn from a genetic study of evolved M mutants (31) suggest that M-M monomer interactions occur among the transmembrane (Tm) domains, whereas higher-order oligomerization of M dimers is governed by the endodomain. The endodomain is also the locus of interactions of M protein with N protein (20-24, 32, 33) and with S protein (34, 35). In order to learn more about intra- and intermolecular interactions of M, we constructed MHV chimeras containing entire or partial substitutions of the SARS-CoV M protein. This strategy allowed us to further define M-N and M-M interactions. Additionally, it revealed that the interactions of M with the E and S proteins are more complex than currently pictured.

MATERIALS AND METHODS

Cells and viruses. MHV-A59 wild-type and mutant virus stocks were grown at 37^{o}C in mouse 17 clone 1 (17Cl1) cells. Plaque titrations and plaque purifications were performed with mouse L2 cells. The host-range chimeric coronavirus designated fMHV.v2 (36), used as the recipient virus for reverse genetics, was grown in feline FCWF cells.

MHV mutant construction. All mutants in this study were isolated by targeted RNA recombination, as described in detail previously (36, 37). Transcription vectors for donor RNA synthesis were constructed from plasmid pSG6X (16), which contains the 3'-most 8.6 kb of the MHV-A59 genome. To create vector pMN1, SARS-CoV domain N3 was transferred to pSG6X from the previously described pMN54-SN3 (15) by transfer of the NheI-BstEII fragment, which runs from

116 the center of the N gene through the start of the 3' UTR. All subsequent constructs containing SARS-
117 CoV domain N3 were then derived from pMN1. Whole or partial SARS-CoV M gene substitutions
118 were made through manipulation of the EcoRV-PspXI fragment running from the end of the E gene
119 through the M gene to the start of the N gene. Chimeric sequences were generated via PCR or two-
120 step PCR using a cloned SARS-CoV M gene cDNA as template (strain Urbani, GenBank accession
121 number AY278741). Alternatively, some M gene fragments were synthesized by PCR from
122 overlapping oligonucleotides and inserted into plasmids using the EagI or BssHII site within M, or
123 else a coding-silent BspEI site that was created at MHV M codons 198 and 199 (equivalent to
124 SARS-CoV M codons 190 and 191). The entire SARS-CoV M substitution in vectors pMN2, pMN3,
125 pMN6, and pMN7 was an exact replacement of the MHV M open reading frame (ORF). The
126 junctions in the partial SARS-CoV M substitutions in vectors pMN4A, pMN4B, pMN4C, pMN5A,
127 pMN5B, pMN8, pMN9, and pMN10 were made at the various boundaries shown in Fig. 1B. The
128 SARS-CoV E gene in vector pMN6, which is an exact ORF-for-ORF replacement, was obtained by
129 transfer from the previously described pLK106 (38) of the SbfI-EcoRV fragment, which runs from
130 immediately downstream of the S gene through the end of the E gene. Similarly, the E gene F20S
131 mutation was placed in vectors pMN5A, pMN5B, pMN7, pMN8, and pMN10 by transfer of an SbfI-
132 EcoRV fragment of cDNA from mutant MN3rev3. Oligonucleotides for PCR and DNA sequencing
133 were obtained from Integrated DNA Technologies. The overall compositions of constructed
134 plasmids were confirmed by restriction analysis, and all ligation junctions and regions generated by
135 PCR amplification were verified by DNA sequencing.

136 The wild-type virus used in this work was Alb741, a recombinant that was previously
137 isolated by targeted RNA recombination with donor RNA from pSG6X (16). For viable chimeric
138 viral mutants, at least three independent isolates were obtained. In each case, once it was established
139 in preliminary experiments that multiple isolates behaved identically, one of them was chosen for

140 further analysis. The exceptions were mutants MN6 and MN7, each of which was isolated only once.
141 Particular chimeric constructs were judged to be lethal after yielding no recombinants in multiple
142 targeted RNA recombination experiments for which parallel positive controls with wild-type donor
143 RNA produced recombinants at a robust frequency.

144 **Virus purification.** Wild-type and mutant MN8 virus were grown in 17Cl1 cell monolayers
145 infected at a multiplicity of 1 PFU/cell. Medium containing released virus was harvested at 14 h
146 postinfection, at a point when monolayers exhibited maximal syncytia formation but minimal lysis
147 or detachment. Virions were purified by polyethylene glycol precipitation followed by equilibrium
148 centrifugation on preformed gradients of 20 to 30% iodixanol (OptPrep, Sigma-Aldrich) in a buffer
149 of 50 mM Tris-maleate (pH 6.5) and 1 mM EDTA. Gradients were centrifuged at 111,000 x *g* in a
150 Beckman SW41 rotor at 4°C for 18 h, and for each, 15 750-µl fractions were collected from the top.

151 **Northern blotting.** RNA was extracted from aliquots of gradient fractions with TRI Reagent
152 (Zymo) according to the manufacturer's instructions. Purified RNA denatured with formaldehyde
153 and formamide was directly dot-blotted onto Nytran Supercharge membranes (Whatman, GE
154 Healthcare) by filtration through a vacuum manifold, followed by UV-crosslinking. Membranes
155 were hybridized with a PCR-amplified probe corresponding to nucleotides 401-909 of the MHV
156 genome, a region unique to genomic (and absent from subgenomic) RNA. The probe was labeled
157 with an AlkPhos Direct kit; blots were visualized using CDP-Star detection reagent (GE Healthcare)
158 and quantitated with a BioRad ChemiDoc XRS+ instrument.

159 **Western blotting.** Purified virions or NP40 lysates prepared from infected 17Cl1 cell
160 monolayers were separated by sodium dodecyl sulfate-polyacrylamide gel electrophoresis (SDS-
161 PAGE) (10%, except where indicated otherwise) and analyzed by Western blotting exactly as
162 described previously (31). Proteins were detected with one of the following: anti-MHV N protein
163 rabbit polyclonal antibody (14); anti-MHV M protein monoclonal antibody J.1.3, generously

provided by John Fleming, University of Wisconsin, Madison; anti-SARS-CoV M protein monoclonal antibody NR-621, similar to 283C (39), obtained through the NIH Biodefense and Emerging Infections Research Resources Repository; or anti-MHV S protein rabbit polyclonal antibody raised against a peptide corresponding to the carboxy-terminal 13 residues of S (DSIVIHNISSHED). Bound antibodies were visualized by enhanced chemiluminescence detection (Pierce), and quantitation was carried with a BioRad ChemiDoc XRS+ instrument.

RESULTS

Construction of an MHV mutant containing the entire SARS-CoV M protein. To more completely elucidate structural protein requirements for coronavirus assembly, we constructed an MHV chimera containing the SARS-CoV M protein. The equivalence of the M endodomain of MHV with that of the very closely related bovine coronavirus was demonstrated in an earlier study (40). However, we anticipated that substitution of the much less homologous SARS-CoV M protein would provide a more stringent test of compatible and incompatible intermolecular interactions. The M proteins of MHV and SARS-CoV, which are lineage A and lineage B betacoronaviruses, respectively, share only 38% amino-acid sequence identity (Fig. 1B). Although M protein is known to engage with each of the other three coronavirus structural proteins, we did not expect that a SARS-CoV M chimera would be significantly hindered in essential M-S or M-E interactions. We had previously found that the SARS-CoV E protein could functionally substitute for MHV E protein (38). Additionally, it was shown that the endodomain of the MHV S protein, the region of S that interacts with M (41, 42), could be completely replaced by its SARS-CoV counterpart (43).

By contrast, we postulated that substitution of a heterologous M protein would require that it

188 be partnered with the region of N protein that assembles with M. Much prior work indicated that N
189 interactions with M are confined to the carboxy-terminal domain of N protein (domain N3) (20-24),
190 which has little or no sequence homology between MHV and SARS-CoV (Fig. 1C). Accordingly,
191 we used targeted RNA recombination (36, 37) to isolate an MHV mutant, MN3, which harbored the
192 complete SARS-CoV M protein as well as domain N3 (plus the adjacent spacer B) of SARS-CoV N
193 protein (Fig 2A). Consistent with our initial assumptions, a chimeric construct that paired the MHV
194 M protein with the SARS-CoV domain N3 (mutant MN1) was lethal, confirming earlier results (15).
195 Likewise, a chimeric construct that paired the SARS-CoV M protein with the MHV domain N3
196 (mutant MN2) was also lethal. These results showed that domain N3 is essential for functional
197 interaction between the coronavirus N and M proteins. Previous work has established that the highly
198 variable spacer B is not essential for virion formation. MHV N spacer B can be altered with
199 divergent coronavirus sequence (44) or an epitope tag (21) or even entirely replaced with a synthetic
200 flexible linker peptide sequence (14). Moreover, the complete deletion of spacer B, in the classical
201 temperature-sensitive mutant Alb4, still allows virion assembly at the permissive temperature (45).
202 Three independent isolates of the MN3 mutant were obtained and their sequences were
203 confirmed. Two of the three contained the exact SARS-CoV M gene sequence. The third isolate had
204 two coding changes in M, N206S and T207A. However, since this virus was phenotypically
205 identical to the other two, these mutations were deemed extraneous, and one (unmutated) isolate was
206 chosen for further study. Notably, none of the MN3 isolates had any sequence changes in the S
207 endodomain, the E gene, or the chimeric N gene. Thus, the substitution of the SARS-CoV M protein
208 did not depend upon the acquisition of second-site mutations in protein domains that interact with M
209 protein, other than N3. To verify expression of proteins encoded by the chimeric virus, lysates from
210 infected cells were analyzed by Western blotting (Fig. 2B). As expected, an anti-SARS-CoV M
211 monoclonal antibody reacted with MN3 M protein but not with wild-type MHV M protein.

Conversely, an anti-MHV M monoclonal antibody reacted with wild-type MHV M protein but not with MN3 M protein. Since the two anti-M antibodies recognize different epitopes, the level of M expression by MN3 could not be directly compared to that of wild type. However, both viruses expressed comparable amounts of wild-type (49.7-kDa) or chimeric (48.3-kDa) N protein, as judged by probing infected cell lysates with polyclonal anti-MHV N antibody. Additionally, as predicted, a monoclonal antibody that recognizes an epitope in wild-type MHV domain N3 (21) did not react with the chimeric MN3 N protein (data not shown).

Although the MN3 mutant was viable, it grew to a ~40-fold lower infectious titer than did wild-type virus and formed smaller plaques at 37°C (Fig. 2C). This plaque size difference was more pronounced at 33°C, and at 39°C MN3 plaques were tiny compared to those of the wild type. This indicated that at least one of the intermolecular interactions of SARS-CoV M protein with MHV components was partially impaired.

Analysis of revertants of MN3. To gain an understanding of the defect in the SARS-CoV M chimera, we isolated mutants with improved growth following 6 to 10 serial passages at 39°C of multiple individual cultures of MN3, each of which had been started from a single plaque. These mutants (referred to as revertants hereafter) formed plaques at 39°C that were markedly larger than those of the MN3 parent but were not fully as large as wild-type plaques. We mapped the mutations that had arisen in each by sequencing the S endodomain and the entire E, M, and N genes. Among 10 independent revertants that were isolated, seven had single changes in the E protein, which localized in either the Tm domain or the endodomain (Fig. 3A). Of the three other revertants, two had mutations in SARS-CoV M (V96L or S172P), and one had a mutation in both S (H1310Y) and N (E146Q). Since most of the reverting mutations fell in E, and since these were in the revertants which formed the largest plaques, this suggested that wild-type MHV E cannot optimally cooperate with SARS-CoV M in virion morphogenesis. Such a finding was unexpected, because we had

236 previously found that the SARS-CoV E protein was nearly completely able to replace the MHV E
237 protein (38).

238 More surprising was that substitution of the entire SARS-CoV E protein in conjunction with
239 the SARS-CoV M protein generated a virus that was further impaired, rather than improved, with
240 respect to MN3. The resulting E-M chimera, MN6, formed very small plaques at 37°C and pinpoint
241 plaques at 39°C (Fig. 3B and C), and it had a ~3-fold lower infectious titer. This unforseen outcome
242 may have been the consequence of distinct activities of the substituted E protein (46) acting in
243 conflict with each other (see Discussion). To ascertain whether alteration of the MHV E protein was
244 sufficient to enhance the fitness of the SARS-CoV M chimera, we reconstructed the mutation from
245 the most robust of the revertants, MN3rev3. The MN7 construct, containing F20S in its E protein,
246 exhibited substantially larger plaques than the MN3 mutant at both 37°C and 39°C (Fig. 3B and C),
247 and it had a 20- to 30-fold higher infectious titer than MN3. This established that the F20S mutation
248 alone is capable of significantly enhancing the growth of the MN3 mutant, suggesting that there
249 exists an interaction between the E and M proteins. However, as MN7 did not entirely recapitulate
250 the phenotype of MN3rev3, we determined the entire genomic sequence of the latter. This revealed
251 four additional mutations in MN3rev3: D42G in nsp2, T298I in nsp15, S163L in the HE pseudogene,
252 and F270V in the S protein ectodomain. We think it likely that none of these points to a previously
253 unknown interaction with M protein, although the S ectodomain mutation conceivably contributed to
254 the larger plaque size of MN3rev3. We therefore included just the E protein F20S mutation in further
255 M chimeric constructs.

256 **Domain substitutions within the M protein.** Multiple lines of evidence from previous
257 structural (30), genetic (31), and virus-like particle studies (47) all suggest that the M protein
258 ectodomain, Tm domains, and endodomain might have separable roles in assembly. To test this
259 notion, we generated intramolecular M protein chimeric substitutions. The first of these, MN8 (Fig.

4A), retained the entire SARS-CoV M protein, except for the restoration of the MHV M ectodomain. The crossover point chosen between MHV and SARS-CoV sequence was a conserved pair of residues (WN) at the junction of the ectodomain and the first Tm domain (Fig. 1B). As with the MN7 construct, the E protein of MN8 incorporated the F20S mutation, and the SARS-CoV domain N3 of N protein. In two additional recombinants, MN9 and MN10 (Fig. 4A), both the MHV ectodomain and Tm domains were restored to the SARS-CoV M protein. In this case, the constructed crossover between MHV and SARS-CoV sequence was a motif (WSFNPETN) occurring shortly after the third Tm domain (Fig. 1B). This motif is highly conserved among all betacoronavirus M proteins, and in MHV it has been shown to be critical for virus-like particle assembly and for virus viability (48). Mutant MN9 was made with the wild-type MHV E protein, while MN10 had the E protein F20S mutation.

The ectodomains of the MHV and SARS-CoV M proteins diverge extensively (Fig. 1B). Moreover, the MHV-A59 M protein ectodomain is O-glycosylated (49), whereas the SARS-CoV M protein ectodomain is N-glycosylated (50). These differences appeared to have no major effect on the growth of MN8 at 37^{o}C (Fig. 4B), relative to that previously seen for the complete SARS-CoV M substitution mutants MN3 and MN7. Likewise, the MN9 and MN10 mutants tolerated the pairing of heterologous Tm and endodomains within the M molecule, indicating that these two regions participate largely independently in intermolecular interactions. Nevertheless, it was noted that at 39^{o}C all three mutants formed smaller plaques than did MN3 or MN7 (data not shown). This impairment was most profound for MN9, suggesting that in MN8 and MN10 the E protein F20S mutation made a beneficial contribution to SARS-CoV M endodomain associations in M protein oligomers.

In contrast to the substitutions that were allowed in MN8, MN9, and MN10, we were not able to subdivide the M protein endodomain in order to define a minimal region capable of

interacting with N protein. Based on prior evidence that the M-N interaction maps to the carboxy terminus of the M endodomain (20, 21, 23, 32), various potential crossover points between the two species of M protein were tested. In constructs MN4A, MN4B, and MN4C, SARS-CoV sequence was grafted onto the tail of the MHV M protein at conserved residues positioned 30 (SGFA), 43 (YK), or 20 (GNY) amino acids, respectively, from the carboxy terminus (Fig. 1B and 4C). Reciprocal substitutions of MHV M sequence on a SARS-CoV M background were also made in constructs MN5A and MN5B. In each case, domain N3 of the N protein was derived from the species corresponding to that of the tail of the M protein. None of these five constructs yielded viable viruses, despite numerous independent trials of targeted RNA recombination, some of which included mutagenized donor RNAs and all of which had robust wild-type controls. The lethality of all of these mutants likely means that, due to the globular nature of the M endodomain, the surface that interacts with domain N3 is more complex than merely a linear stretch of primary sequence.

Analysis of virions of the SARS-CoV M protein chimera. We consistently noted that monolayers inoculated at 37°C with MN3 or MN8 exhibited a progression of syncytia formation and cytopathic effect similar to monolayers inoculated with wild-type virus at the same multiplicity of infection. However, virus released from cells infected with either of these SARS-CoV M chimeras had a markedly lower infectious titer than wild type. Moreover, preliminary evidence showed that virions of MN3 and MN8 were defective in the selective packaging of genomic RNA (L. Kuo and P. S. Masters, unpublished data), suggesting a possible basis for their reduced infectivity. These observations prompted us to examine SARS-CoV M chimeric virions in more detail. We chose MN8 for this analysis because its composition would allow us to directly compare M protein in wild-type and mutant virions using an anti-M monoclonal antibody that recognizes the MHV M protein ectodomain (40).

Virions of MN8 and wild type were purified by equilibrium centrifugation on continuous

gradients of 20 to 30% iodixanol and collected in multiple fractions that were analyzed for infectivity, viral protein, and genomic RNA (Fig. 5). One readily apparent distinction between the two viruses was that they had markedly different buoyant densities. This difference was confirmed by the nearly identical density profiles of the two gradients shown in Fig. 5A. MN8 and wild-type virions were also seen to sediment differently in glycerol-tartrate gradients (41) and in iodixanol gradients of other densities (data not shown). A second salient contrast between the two viruses was that the MN8 mutant had a severely reduced infectious titer, nearly 30-fold lower than that of the wild type (Fig. 5A and F). However, this deficiency was not due to a decreased quantity of assembled viral particles. The levels of N and M proteins detected by Western blotting were comparable for MN8 and wild-type virions, and the two had similar ratios of N protein to M protein (Fig. 5B, C, and F). Additionally, contrary to our original expectations, there was no impairment in the amount of genomic RNA packaged by the mutant. Indeed, virions of MN8 contained slightly more genomic RNA than wild-type virions (Fig. 5D-F), and Northern blotting verified that MN8 genomic RNA was intact (data not shown). For both mutant and wild type, the peaks of protein and RNA coincided with the respective peaks of infectivity. This indicated that MN8 virions did not consist of separate pools of empty and RNA-containing particles.

Surprisingly, MN8 virions contained drastically reduced amounts of S protein compared to wild-type virions. MHV S protein is synthesized as a 180-kDa glycoprotein, S_0, that is cleaved by cellular proteases into amino- and carboxy-terminal halves, S_1 and S_2. Using an antibody specific for the carboxy terminus of the molecule, we observed that S in wild-type virions was almost entirely in the cleaved S_2 form, although trace amounts of S_0 were seen as well (Fig. 6A). By contrast, only minor quantities of S_2 were detected in MN8 virions. Since S is essential for the initiation of infection, this accounted for the diminished infectivity of the M chimera. This difference in MN8 was not due to a failure to synthesize S. Examination of lysates of infected cells showed that wild

type and MN8 expressed equivalent amounts of S protein, and intracellular S was almost all in the uncleaved S_0 form (Fig. 6B). We also separated virions in a higher-density SDS-PAGE gel to look for evidence of degradation of S protein, analogous to that described for an E protein mutant of IBV (51). This revealed a minor amount of a 12.5-kDa carboxy-terminal fragment of S protein in wild-type virions, corresponding to roughly 110 amino acids, which would comprise heptad-repeat region 2, the Tm domain, and the endodomain (Fig. 6C). However, no such membrane-bound remnant of S was found in MN8 virions, although we would have expected it to be abundant if S had been incorporated into mutant virions and then degraded. Our results therefore indicated that, even though adequate amounts of MHV S protein were available, they were not efficiently incorporated into assembling virions by SARS-CoV M protein. To determine if this was a general characteristic of the SARS-CoV M protein chimeras, we grew separate stocks of wild-type, MN8, MN3, and MN3rev3 viruses and purified them on continuous iodixanol gradients. Equivalent quantities of virions, as judged by N protein content, were analyzed for S protein. As shown in Fig. 6D, virions of the original chimera, MN3, had even more severely reduced incorporation of S protein than did MN8. By contrast, the large-plaque revertant MN3rev3 had levels of S protein approaching those of the wild type. Thus, the levels of S protein incorporation into various SARS-CoV M protein chimeras was consistent with their relative titers with respect to that of the wild type. To attempt to remedy this defect, we designed an additional chimeric construct, MN11 (Fig. 6E). This mutant incorporated the SARS-CoV S protein Tm and endodomain, in addition to the M, N, and E substitutions already made in MN8. Remarkably, this modification further impaired the virus, since MN11 was lethal. In eight independent targeted RNA recombination trials no recombinants were obtained with MN11 donor RNA, whereas wild-type control RNA samples in the same experiments yielded robust numbers of recombinants. Contrary to expectations, the inclusion of the SARS-CoV homolog of the region of S protein known to directly interact with the M endodomain was not sufficient to rescue

normally assembled viruses. This suggests that there exist structural protein interactions or host cell-specific interactions that remain unaccounted for in coronavirus virion morphogenesis.

DISCUSSION

The construction of interspecies chimeras has proven valuable in the identification of intra- and intermolecular interactions of the coronavirus N protein (15, 16, 19, 44). We have now applied this approach to the M protein. It was previously found that substitution of the highly homologous BCoV M protein endodomain had no discernable effect on MHV (40). In the present study, we extended this test over a significantly greater phylogenetic distance, by creating substitutions of SARS-CoV M sequence in MHV. This has sharpened our picture of the interaction of M with itself and with N protein, and it has revealed unanticipated complexities of the interactions of M with the E and S proteins.

M-N and M-M interactions. Our isolation of the chimera MN3 made clear that incorporation of the heterologous SARS-CoV M protein into MHV required the concomitant inclusion of the SARS-CoV N protein carboxy-terminal domain N3 (Fig. 2). Chimeras MN1 and MN2, containing just one or the other of these components, were not viable. Moreover, analysis of the chimera MN8 showed that its virions contained abundant amounts of N and M proteins in a ratio comparable to that of wild-type virions (Fig. 5). Together, these results demonstrated that domain N3 is both necessary and sufficient for N protein to interact with M protein in virus assembly. This conclusion conforms with most previous genetic and molecular biological studies (20-24). The necessity of domain N3 for virion assembly also explains why intracellular carboxy-terminal truncated forms of N protein, likely generated by caspases late in infection (52, 53), are not

incorporated into released virions. The sufficiency of N3 accords well with cryo-EM and tomographic reconstructions of MHV and SARS-CoV virions, which found the M endodomain to be connected to the nucleocapsid via a single "thread-like" connection (54, 55). Nevertheless, some work has purported to detect essential interactions with M that map to parts of N protein other than N3. A mammalian two-hybrid analysis of SARS-CoV N and M localized the interacting segment of N to a region comprising the downstream end of the NTD and all of the SR region (25). Another study used GST pull-down assays to map the SARS-CoV N-M interaction to a segment of N encompassing the linker between the SR region and the CTD (26). Finally, an analysis of SARS-CoV M and N proteins found the carboxy terminus of N to be required for formation of virus-like particles with M, but proposed an additional M-binding site falling in the center of the NTD (27). The biological relevance of any of these latter reported interactions remains to be determined, but our results establish that they are not required for virion assembly.

Beyond substitution of the entire SARS-CoV M protein in MHV, we found that it was possible to construct functional chimeric viruses in which intramolecular M protein substitutions were made (Fig. 4). In the chimera MN8, the ectodomain of MHV M was linked to the Tm domains and endodomain of SARS-CoV M. This substitution mutant was nearly as robust as the complete M protein chimera MN3. Such an outcome was not unexpected, because the M ectodomain varies considerably among different strains of MHV, and it is relatively tolerant to mutation (40). Additionally, the MHV ectodomain, which is normally O-glycosylated, can be altered to either an unglycosylated or an N-glycosylated form without affecting virus growth in tissue culture (56). Our replacement of the N-glycosylated SARS-CoV M ectodomain with its O-glycosylated MHV M counterpart provides further support that the mode of M protein glycosylation is not a crucial factor in virion assembly.

A more extensive intramolecular substitution was made in mutants MN9 and MN10, in

404 which the ectodomain and Tm domains of MHV M were linked to the endodomain of SARS-CoV M
405 (Fig. 4). The viability of these constructs suggests that folding and oligomerization of the M protein
406 Tm domains and the endodomain, for the most part, occur independently of one another. This
407 conclusion is consistent with our previous finding of truncated endodomain variants of the M
408 protein, designated M*, that evolved by gene duplication in MHV E-deletion mutants to compensate
409 for the absence of E protein (31). Similar M* proteins have very recently been observed to arise
410 upon passaging of SARS-CoV E-deletion mutants, also (57). The MHV M* protein was found to be
411 incorporated into purified virions, which showed that interactions among Tm domains were
412 sufficient to sustain the assembly of M* with native M protein. Conversely, cryo-EM analyses of
413 coronavirus virions resolved the basic unit of M as a dimer, and intermolecular contacts in higher-
414 order oligomers were seen to occur exclusively between M endodomains (30). Thus, the MN9 and
415 MN10 chimeras demonstrate that these two classes of interactions can even be apportioned between
416 M Tm and endodomains derived from two divergent coronavirus species.

417 Although the M protein could be partitioned at domain boundaries, we were not able to
418 further dissect the M endodomain to identify a short linear segment functionally analogous to
419 domain N3 of N protein. Various considerations had indicated that this ought to be possible. First, an
420 early characterization of M protein showed that roughly 15 carboxy-terminal residues were
421 susceptible to protease digestion, which was taken to mean that the carboxy terminus of M was
422 structurally separate from the rest of the globular endodomain (28, 29). Second, prior genetic studies
423 mapped a dominant role in the MHV M-N interaction to an electrostatic bridge between the
424 penultimate M residue, R227, and residues D440 and D441 in domain N3 (20-23). Additionally, *in*
425 *vitro* assays with TGEV (32) and SARS-CoV (33) M protein fragments also appeared to localize the
426 N-binding component of M to within 30 residues of the carboxy terminus. However, our multiple
427 attempts to obtain chimeric recombinants with crossover sites chosen at distinct motifs near the

carboxy terminus of either SARS-CoV or MHV M protein were uniformly unsuccessful (Fig. 4C). This negative result accords well with previous findings that the mutations in several second-site revertants of defective MHV M or N assembly mutants mapped to positions considerably upstream in the M endodomain (20, 21, 23). Moreover, it was pointed out previously that, in many cases, the identical upstream mutation in the M endodomain was independently isolated either as an intragenic suppressor of certain R227 M protein mutants or as an intergenic suppressor of a D440/D441 N mutant (23). This convergence presents a strong argument that direct or indirect contributions are made by upstream regions of the M endodomain to the interaction with N protein. Further evidence for a larger participation of the endodomain comes from cryo-EM reconstructions showing that virion M protein endodomains exist in either a compact form or an extended form, with only the latter making contact with the nucleocapsid (30). This suggests that binding to domain N3 induces a conformational change affecting the entire M endodomain. Since domain N3 is intrinsically disordered (18) we envision that it fits into a surface on the globular M endodomain composed of residues that are discontiguous in the primary sequence. More detailed exploration of this interaction would benefit greatly from higher-resolution structural information on the M endodomain, which is as yet unavailable.

M-E and M-S interactions. At the outset of this study, we assumed that interactions with MHV E or S would not be affected by the SARS-CoV M protein substitution. Nevertheless, despite the complete reconstitution of the M-N interaction in chimeric viruses, the transplanted SARS-CoV M protein did not perform well with the other two structural proteins of MHV. In a previous study, we showed that the SARS-CoV E protein could efficiently replace the MHV E protein (38), which seemed to imply that the reciprocal pairing of MHV E with SARS-CoV M would be equally robust. However, the marked temperature-sensitivity of the original M chimera MN3 was found to be partially suppressed by mutations in the MHV E protein (Fig. 3). Although there is extensive

452 evidence for colocalization and association of M and E in infected cells (8, 58), this is the first
453 observed instance of genetic cross-talk between the M and E proteins. Previously, only intragenic
454 revertants of E mutants had been isolated (38, 59-61). This finding suggested that the SARS-CoV M
455 protein would ideally require its homologous E partner. Paradoxically, though, substitution of the
456 entire SARS-CoV E protein in mutant MN6 was deleterious, rather than beneficial (Fig. 3).

457 E protein is known to have at least three separate functions. First, it promotes the assembly of
458 virions, specifically through mediating aggregation-prone M-M interactions in the membrane of the
459 budding compartment (6). Second, it triggers disassembly of the Golgi, which somehow facilitates
460 the cellular egress of assembled virions (51, 62, 63). Third, E associates with host factors, thereby
461 affecting cell signaling and viral pathogenesis (64, 65). The first two of these functions, virion
462 assembly and Golgi-disruption, are carried out by distinct oligomeric states of the E molecule (46).
463 The third role is the only one that has yet been shown to depend on the ion channel activity of E
464 protein (61). Not all functions of E protein appear to be required by all coronaviruses. The
465 consequences of deletion of the E gene were seen to vary from modest impairment for SARS-CoV
466 (66) to severe impairment for MHV (38, 67) to lethality for TGEV and MERS-CoV (68, 69); also,
467 for SARS-CoV the E-deletion phenotype was dependent on cell type. The multiplicity of roles of E
468 protein likely explains why we were previously able to substitute the phylogenetically distant E
469 proteins of SARS-CoV or IBV for that of MHV, but, on the other hand, the TGEV E protein was
470 inert in an MHV background (38). Thus, some functions of E may be interchangeable between a
471 given pair of coronaviruses, while others are not. It is therefore conceivable that transplanting the
472 SARS-CoV M protein into MHV placed it in a heterologous environment where neither MHV E nor
473 SARS-CoV E could simultaneously (i) address the requirements of M protein and (ii) interact with
474 cellular components in a manner optimal for productive infection.

475 More enigmatic than the M-E interaction was the defective M-S interaction in the SARS-

476 CoV M chimera. Our analysis of the MN8 mutant revealed that virions of the chimera had a striking
477 deficiency of S protein, and consequently, a much higher particle-to-PFU ratio than wild type (Fig.
478 6). MN8 virions also had a lower buoyant density than wild-type virions (Fig. 5), which may be
479 attributed to the lack of S or may point to some as yet uncharacterized defect in virion
480 morphogenesis in the chimera. There is ample evidence that M protein has the sole responsibility for
481 recruiting S protein into virions (9, 10) through interactions that localize to the endodomain of S (41,
482 42). One possible reason for the reduced complement of S protein in MN8 could be that the SARS-
483 CoV M protein cannot efficiently bind to the MHV S endodomain. This seems unlikely, given that
484 the opposite arrangement is fully functional. Previous work showed that the SARS-CoV S protein
485 Tm and endodomain were completely able to replace their MHV S counterpart (43, 70).
486 Additionally, a foreign membrane protein harboring the SARS-CoV S Tm and endodomain was
487 incorporated into MHV virions with slightly higher efficiency than the MHV version of the same
488 protein (43). Moreover, if the carboxy terminus of MHV S was incompatible with SARS-CoV M,
489 then the defect in the MN8 mutant should have been repaired by substitution of the SARS-CoV S
490 Tm and endodomain. Surprisingly, the chimeric construct containing that substitution (MN11) was
491 lethal.

492 A second possible cause of the sparse incorporation of S protein into MN8 virions could be
493 that despite being well able to interact, the two proteins colocalize too briefly to do so efficiently. It
494 has been shown that the terminus of the SARS-CoV S endodomain contains a COPI-binding KxHxx
495 motif that is thought to be responsible for recycling of S protein from the Golgi back to the ER, thus
496 increasing the time S spends in the proximity of M protein (71). The MHV S protein endodomain
497 does not possess such a signal, although this lack does not impede its ability to interact with the
498 MHV M protein. Again, if this constituted a deficiency in MN8 with respect to S protein contacting
499 the SARS-CoV M protein, then it should have been rescued by the SARS-CoV S endodomain

substitution in the MN11 chimera. Finally, we could find no evidence that MHV S protein was incorporated into MN8 virions but subsequently degraded, as was found to happen with a particular E protein mutant of IBV (51). Thus, further work will be required to unravel the complete range of intermolecular interactions in which the coronavirus M protein participates.

ACKNOWLEDGMENTS

We thank the Applied Genomics Technology and Bioinformatics Core Facilities of the Wadsworth Center for Sanger and Next Generation DNA sequencing and genomic sequence analysis. We thank the NIH Biodefense and Emerging Infections Research Resources Repository for providing anti-SARS-CoV M protein monoclonal antibody.

This work was supported by National Institutes of Health (National Institute of Allergy and Infectious Diseases) grant R01 AI064603.

REFERENCES

1. **Masters PS, Perlman S.** 2013. Coronaviridae. p 825-858. *In* Knipe DM, Howley PM, Cohen, JI, Griffin DE, Lamb RA, Martin MA, Racaniello VR, Roizman B (ed), Fields Virology, 6th ed, vol 1. Lippincott Williams & Wilkins, Philadelphia, PA.
2. **Perlman S, Netland J.** 2009. Coronaviruses post-SARS: update on replication and pathogenesis. Nat. Rev. Microbiol. **7:**439-450.
3. **Vennema H, Godeke GJ, Rossen JW, Voorhout WF, Horzinek MC, Opstelten DJ, Rottier PJ.** 1996. Nucleocapsid-independent assembly of coronavirus-like particles by co-expression of viral envelope protein genes. EMBO J. **15:**2020-2028.
4. **Bos EC, Luytjes W, van der Meulen HV, Koerten HK, Spaan WJ.** 1996. The production of recombinant infectious DI-particles of a murine coronavirus in the absence of helper virus. Virology **218:**52-60.
5. **Corse E, Machamer CE.** 2000. Infectious bronchitis virus E protein is targeted to the Golgi complex and directs release of virus-like particles. J. Virol. **74:**4319-4326.
6. **Boscarino JA, Logan HL, Lacny JJ, Gallagher TM.** 2008. Envelope protein palmitoylations are crucial for murine coronavirus assembly. J. Virol. **82:**2989-2999.
7. **Siu YL, Teoh KT, Lo J, Chan CM, Kien F, Escriou N, Tsao SW, Nicholls JM, Altmeyer R, Peiris JS, Bruzzone R, Nal B.** 2008. The M, E, and N structural proteins of the severe acute respiratory syndrome coronavirus are required for efficient assembly, trafficking, and release of virus-like particles. J. Virol. **82:**11318-11330.
8. **Venkatagopalan P, Daskalova SM, Lopez LA, Dolezal KA, Hogue BG.** 2015. Coronavirus envelope (E) protein remains at the site of assembly. Virology **478:**75-85.
9. **Opstelten DJ, Raamsman MJ, Wolfs K, Horzinek MC, Rottier PJ.** 1995. Envelope glycoprotein interactions in coronavirus assembly. J. Cell Biol. **131:**339-349.
10. **Nguyen VP, Hogue BG.** 1997. Protein interactions during coronavirus assembly. J. Virol. **71:**9278-9284.
11. **Holmes KV, Dollar EW, Sturman LS**. 1981. Tunicamycin resistant glycosylation of a coronavirus glycoprotein: demonstration of a novel type of viral glycoprotein. Virology **115:**334-344.
12. **Rottier PJM, Horzinek MC, van der Zeijst BAM.** 1981. Viral protein synthesis in mouse hepatitis virus strain A59-infected cells: effects of tunicamycin. J. Virol. **40:**350-357.
13. **Chang CK, Hou MH, Chang CF, Hsiao CD, Huang TH.** 2014. The SARS coronavirus nucleocapsid protein – forms and functions. Antiviral Res. **103:**39-50.
14. **Hurst KR, Koetzner CA, Masters PS.** 2009. Identification of in vivo-interacting domains of the murine coronavirus nucleocapsid protein. J. Virol. **83:**7221-7234.
15. **Hurst KR, Ye R, Goebel SJ, Jayaraman P, Masters PS.** 2010. An interaction between the nucleocapsid protein and a component of the replicase-transcriptase complex is crucial for the infectivity of coronavirus genomic RNA. J. Virol. **84:**10276-10288.
16. **Kuo L, Koetzner CA, Hurst KR, Masters PS.** 2014. Recognition of the murine coronavirus genomic RNA packaging signal depends on the second RNA-binding domain of the nucleocapsid protein. J. Virol. **88:**4451-4465.
17. **Chang CK, Chen CM, Chiang MH, Hsu YL, Huang TH.** 2013. Transient oligomerization of the SARS-CoV N protein – implication for virus ribonucleoprotein packaging. PLoS One **8:**e65045.
18. **Chang CK, Hsu YL, Chang YH, Chao FA, Wu MC, Huang YS, Hu CK, Huang TH.** 2009. Multiple nucleic acid binding sites and intrinsic disorder of severe acute respiratory

syndrome coronavirus nucleocapsid protein: implications for ribonucleocapsid protein packaging. J. Virol. **83:**2255-2264.

19. **Hurst KR, Koetzner CA, Masters PS.** 2013. Characterization of a critical interaction between the coronavirus nucleocapsid protein and nonstructural protein 3 of the viral replicase-transcriptase complex. J. Virol. **87:**9159-9172.
20. **Kuo L, Masters PS**. 2002. Genetic evidence for a structural interaction between the carboxy termini of the membrane and nucleocapsid proteins of mouse hepatitis virus. J. Virol. **76:**4987-4999.
21. **Hurst KR, Kuo L, Koetzner CA, Ye R, Hsue B, Masters PS.** 2005. A major determinant for membrane protein interaction localizes to the carboxy-terminal domain of the mouse coronavirus nucleocapsid protein. J. Virol. **79:**13285-13297.
22. **Verma S, Bednar V, Blount A, Hogue BG.** 2006. Identification of functionally important negatively charged residues in the carboxy end of mouse hepatitis coronavirus A59 nucleocapsid protein. J. Virol. **80:**4344-4355.
23. **Verma S, Lopez LA, Bednar V, Hogue BG.** 2007. Importance of the penultimate positive charge in mouse hepatitis coronavirus A59 membrane protein. J. Virol. **81:**5339-5348.
24. **Luo H, Wu D, Shen C, Chen K, Shen X, Jiang H.** 2006. Severe acute respiratory syndrome coronavirus membrane protein interacts with nucleocapsid protein mostly through their carboxyl termini by electrostatic attraction. Int. J. Biochem. Cell Biol. **38:**589-599.
25. **He R, Leeson A, Ballantine M, Andonov A, Baker L, Dobie F, Li Y, Bastien N, Feldmann H, Strocher U, Theriault S, Cutts T, Cao J, Booth TF, Plummer FA, Tyler S, Li X.** 2004. Characterization of protein-protein interactions between the nucleocapsid protein and membrane protein of the SARS coronavirus. Virus Res. **105:**121-125.
26. **Fang X, Ye LB, Zhang Y, Li B, Li S, Kong L, Wang Y, Zheng H, Wang W, Wu Z.** 2006. Nucleocapsid amino acids 211 to 254, in particular, tetrad glutamines, are essential for the interaction between the nucleocapsid and membrane proteins of SARS-associated coronavirus. J. Microbiol. **44:**577-580.
27. **Hatakeyama S, Matsuoka Y, Ueshiba H, Komatsu N, Itoh K, Shichijo S, Kanai T, Fukushi M, Ishida I, Kirikae T, Sasazuki T, Miyoshi-Akiyama T.** 2008. Dissection and identification of regions required to form pseudoparticles by the interaction between the nucleocapsid (N) and membrane (M) proteins of SARS coronavirus. Virology **380:**99-108.
28. **Rottier P, Brandenburg D, Armstrong J, van der Zeijst B, Warren G.** 1984. Assembly in vitro of a spanning membrane protein of the endoplasmic reticulum: the E1 glycoprotein of coronavirus mouse hepatitis virus A59. Proc. Natl. Acad. Sci. USA **81:**1421-1425.
29. **Rottier PJ, Welling GW, Welling-Wester S, Niesters HG, Lenstra JA, Van der Zeijst BA.** 1986. Predicted membrane topology of the coronavirus protein E1. Biochemistry **25:**1335-1339.
30. **Neuman BW, Kiss G, Kunding AH, Bhella D, Baksh MF, Connelly S, Droese B, Klaus JP, Makino S, Sawicki SG, Siddell SG, Stamou DG, Wilson IA, Kuhn P, Buchmeier MJ.** 2011. A structural analysis of M protein in coronavirus assembly and morphology. J. Struct. Biol. **174:**11-22.
31. **Kuo L, Masters PS.** 2010. Evolved variants of the membrane protein can partially replace the envelope protein in murine coronavirus assembly. J. Virol. **84:**12872-12885.
32. **Escors D, Ortego J, Laude H, Enjuanes L.** 2001. The membrane M protein carboxy terminus binds to transmissible gastroenteritis coronavirus core and contributes to core stability. J. Virol. **75:**1312-1324.
33. **Fang X, Ye L, Timani KA, Li S, Zen Y, Zhao M, Zheng H, Wu Z.** 2005. Peptide domain

involved in the interaction between membrane protein and nucleocapsid protein of SARS-associated coronavirus. J. Biochem. Mol. Biol. **38:**381-385.

34. **de Haan CA, Smeets M, Vernooij F, Vennema H, Rottier PJ.** 1999. Mapping of the coronavirus membrane protein domains involved in interaction with the spike protein. J. Virol. **73:**7441-7452.

35. **McBride CE, Machamer CE.** 2010. A single tyrosine in the severe acute respiratory syndrome coronavirus membrane protein cytoplasmic tail is important for efficient interaction with spike protein. J. Virol. 84:1891-1901.

36. **Goebel SJ, Hsue B, Dombrowski TF, Masters PS.** 2004. Characterization of the RNA components of a putative molecular switch in the 3' untranslated region of the murine coronavirus genome. J. Virol. **78:**669-682.

37. **Kuo L, Godeke GJ, Raamsman MJ, Masters PS, Rottier PJ.** 2000. Retargeting of coronavirus by substitution of the spike glycoprotein ectodomain: crossing the host cell species barrier. J. Virol. **74:**1393-1406.

38. **Kuo L, Hurst KR, Masters PS.** 2007. Exceptional flexibility in the sequence requirements for coronavirus small envelope protein function. J. Virol. **81:**2249-2262.

39. **Tripp RA, Haynes LM, Moore D, Anderson B, Tamin A, Harcourt BH, Jones LP, Yilla M, Babcock GJ, Greenough T, Ambrosino DM, Alvarez R, Callaway J, Cavitt S, Kamrud K, Alterson H, Smith J, Harcourt JL, Miao C, Razdan R, Comer JA, Rollin PE, Ksiazek TG, Sanchez A, Rota PA, Bellini WJ, Anderson LJ.** 2005. Monoclonal antibodies to SARS-associated coronavirus (SARS-CoV): identification of neutralizing and antibodies reactive to S, N, M and E viral proteins. J Virol. Methods **128:**21-28.

40. **de Haan CA, Kuo L, Masters PS, Vennema H, Rottier PJ.** 1998. Coronavirus particle assembly: primary structure requirements of the membrane protein. J. Virol. **72:**6838-6850.

41. **Ye R, Montalto-Morrison C, Masters PS.** 2004. Genetic analysis of determinants for spike glycoprotein assembly into murine coronavirus virions: distinct roles for charge-rich and cysteine-rich regions of the endodomain. J. Virol. **78:**9904-9917.

42. **Bosch BJ, de Haan CA, Smits SL, Rottier PJ.** 2005. Spike protein assembly into the coronavirion: exploring the limits of its sequence requirements. Virology **334:**306-318.

43. **Yao Q, Masters PS, Ye R.** 2013. Negatively charged residues in the endodomain are critical for specific assembly of spike protein into murine coronavirus. Virology **442:**74-81.

44. **Peng D, Koetzner CA, McMahon T, Zhu Y, Masters PS.** 1995. Construction of murine coronavirus mutants containing interspecies chimeric nucleocapsid proteins. J. Virol. **69:**5475-5484.

45. **Koetzner CA, Parker MM, Ricard CS, Sturman LS, Masters PS.** 1992. Repair and mutagenesis of the genome of a deletion mutant of the coronavirus mouse hepatitis virus by targeted RNA recombination. J. Virol. **66:**1841-1848.

46. **Westerbeck JW, Machamer CE.** 2015. A coronavirus E protein is present in two distinct pools with different effects on assembly and the secretory pathway. J. Virol. **89:**9313-9323

47. **de Haan CA, Vennema H, Rottier PJ.** 2000. Assembly of the coronavirus envelope: homotypic interactions between the M proteins. J. Virol. **74:**4967-4978.

48. **Arndt AL, Larson BJ, Hogue BG.** 2010. A conserved domain in the coronavirus membrane protein tail is important for virus assembly. J. Virol. **84:**11418-11428.

49. **Niemann H, Geyer R, Klenk HD, Linder D, Stirm S, Wirth M.** 1984. The carbohydrates of mouse hepatitis virus (MHV) A59: structures of the O-glycosidically linked oligosaccharides of glycoprotein E1. EMBO J. **3:**665-670.

50. **Oostra M, de Haan CA, de Groot RJ, Rottier PJ.** 2006. Glycosylation of the severe acute

655 respiratory syndrome coronavirus triple-spanning membrane proteins 3a and M. J. Virol.
656 **80:**2326-2336.
657 51. **Machamer CE, Youn S.** 2006. The transmembrane domain of the infectious bronchitis virus
658 E protein is required for efficient virus release. Adv. Exp. Med. Biol. **581:**193-198.
659 52. **Eléouët JF, Slee EA, Saurini F, Castagné N, Poncet D, Garrido C, Solary E, Martin SJ.**
660 2000. The viral nucleocapsid protein of transmissible gastroenteritis coronavirus (TGEV) is
661 cleaved by caspase-6 and -7 during TGEV-induced apoptosis. J. Virol. **74:**3975-3983.
662 53. **Diemer C, Schneider M, Seebach J, Quaas J, Frösner G, Schätzl HM, Gilch S.** 2008.
663 Cell type-specific cleavage of nucleocapsid protein by effector caspases during SARS
664 coronavirus infection. J. Mol. Biol. **376:**23-34.
665 54. **Neuman BW, Adair BD, Yoshioka C, Quispe JD, Orca G, Kuhn P, Milligan RA, Yeager**
666 **M, Buchmeier MJ.** 2006. Supramolecular architecture of severe acute respiratory syndrome
667 coronavirus revealed by electron cryomicroscopy. J. Virol. **80:**7918-7928.
668 55. **Bárcena M, Oostergetel GT, Bartelink W, Faas FG, Verkleij A, Rottier PJ, Koster AJ,**
669 **Bosch BJ.** 2009. Cryo-electron tomography of mouse hepatitis virus: Insights into the
670 structure of the coronavirion. Proc. Natl. Acad. Sci. USA. **106:**582-587.
671 56. **de Haan CA, de Wit M, Kuo L, Montalto-Morrison C, Haagmans BL, Weiss SR,**
672 **Masters PS, Rottier PJ.** 2003. The glycosylation status of the murine hepatitis coronavirus
673 M protein affects the interferogenic capacity of the virus in vitro and its ability to replicate in
674 the liver but not the brain. Virology **312:**395-406.
675 57. **Jimenez-Guardeño JM, Regla-Nava JA, Nieto-Torres JL, DeDiego ML, Castaño-**
676 **Rodriguez C, Fernandez-Delgado R, Perlman S, Enjuanes L.** 2015. Identification of the
677 mechanisms causing reversion to virulence in an attenuated SARS-CoV for the design of a
678 genetically stable vaccine. PLoS Pathog. **11:**e1005215.
679 58. **Corse E, Machamer CE.** 2003. The cytoplasmic tails of infectious bronchitis virus E and M
680 proteins mediate their interaction. Virology **312:**25-34.
681 59. **Fischer F, Stegen CF, Masters PS, Samsonoff WA.** 1998. Analysis of constructed E gene
682 mutants of mouse hepatitis virus confirms a pivotal role for E protein in coronavirus
683 assembly. J.Virol. **72:**7885-7894.
684 60. **Ye Y, Hogue BG.** 2007. Role of the coronavirus E viroporin protein transmembrane domain
685 in virus assembly. J. Virol. **81**:3597-3607.
686 61. **Nieto-Torres JL, DeDiego ML, Verdiá-Báguena C, Jimenez-Guardeño JM, Regla-Nava**
687 **JA, Fernandez-Delgado R, Castaño-Rodriguez C, Alcaraz A, Torres J, Aguilella VM,**
688 **Enjuanes L.** 2014. Severe acute respiratory syndrome coronavirus envelope protein ion
689 channel activity promotes virus fitness and pathogenesis. PLoS Pathog. **10:**e1004077.
690 62. **Ruch TR, Machamer CE.** 2011. The hydrophobic domain of infectious bronchitis virus E
691 protein alters the host secretory pathway and is important for release of infectious virus. J.
692 Virol. **85:**675-685.
693 63. **Ruch TR, Machamer CE.** 2012. A single polar residue and distinct membrane topologies
694 impact the function of the infectious bronchitis coronavirus E protein. PLoS Pathog.
695 **8:**e1002674.
696 64. **Teoh KT, Siu YL, Chan WL, Schlüter MA, Liu CJ, Peiris JS, Bruzzone R, Margolis B,**
697 **Nal B.** 2010. The SARS coronavirus E protein interacts with PALS1 and alters tight junction
698 formation and epithelial morphogenesis. Mol. Biol. Cell **21:**3838-3852.
699 65. **Jimenez-Guardeño JM, Nieto-Torres JL, DeDiego ML, Regla-Nava JA, Fernandez-**
700 **Delgado R, Castaño-Rodriguez C, Enjuanes L.** 2014. The PDZ-binding motif of severe
701 acute respiratory syndrome coronavirus envelope protein is a determinant of viral

pathogenesis. PLoS Pathog. **10:**e1004320.

66. **DeDiego ML, Alvarez E, Almazán F, Rejas MT, Lamirande E, Roberts A, Shieh WJ, Zaki SR, Subbarao K, Enjuanes L.** 2007. A severe acute respiratory syndrome coronavirus that lacks the E gene is attenuated in vitro and in vivo. J. Virol. **81:**1701-1713.
67. **Kuo L, Masters PS**. 2003. The small envelope protein E is not essential for murine coronavirus replication. J. Virol. **77:**4597-4608.
68. **Ortego J, Ceriani JE, Patiño C, Plana J, Enjuanes L.** 2007. Absence of E protein arrests transmissible gastroenteritis coronavirus maturation in the secretory pathway. Virology **36:**296-308.
69. **Almazán F, DeDiego ML, Sola I, Zuñiga S, Nieto-Torres JL, Marquez-Jurado S, Andrés G, Enjuanes L.** 2013. Engineering a replication-competent, propagation-defective Middle East respiratory syndrome coronavirus as a vaccine candidate. MBio. **4:**e00650.
70. **Lokugamage KG, Yoshikawa-Iwata N, Ito N, Watts DM, Wyde PR, Wang N, Newman P, Kent Tseng CT, Peters CJ, Makino S.** 2008. Chimeric coronavirus-like particles carrying severe acute respiratory syndrome coronavirus (SCoV) S protein protect mice against challenge with SCoV. Vaccine **26:**797-808.
71. **McBride CE, Li J, Machamer CE.** 2007. The cytoplasmic tail of the severe acute respiratory syndrome coronavirus spike protein contains a novel endoplasmic reticulum retrieval signal that binds COPI and promotes interaction with membrane protein. J. Virol. **81:**2418-2428.

FIGURE LEGENDS

FIG 1 Coronavirus M and N protein domain structure. (A) Schematics of the M and N proteins, with summary of currently assigned interactions. *Tm*, transmembrane domain; *NTD (N1b)*, amino-terminal RNA-binding domain; *SR*, serine- and arginine-rich region; *CTD (N2b)*, carboxy-terminal RNA-binding domain; *B*, spacer region; *N3*, carboxy-terminal domain. (B) Alignment of the MHV and SARS-CoV M proteins. Tm domains are as modeled in Rottier et al. (29). Vertical bars between the ectodomain, Tm domains, and endodomain indicate functional crossover boundaries in constructed chimeras; filled circles denote nonfunctional crossover boundaries within the M endodomain. (C) Alignment of the carboxy termini of the MHV and SARS-CoV N proteins. The vertical bar indicates the functional crossover boundary in chimeras; broken line indicates the boundary between spacer B and domain N3. GenBank accession numbers for the sequences shown are: MHV-A59, AY700211; and SARS-CoV strain Urbani, AY278741.

FIG 2 Construction of an MHV chimera containing the entire M protein of SARS-CoV. (A) Schematics of wild-type virus and chimeras MN1, MN2, and MN3 containing mutant M and N proteins. Shading represents SARS-CoV sequence substituted for that of MHV. (B) Western blots of lysates from mouse 17Cl1 cells infected with wild-type MHV or MN3 virus; *mock*, uninfected 17Cl1 cells. Additional controls, designated mock (V) and SCoV (V), were protein fractions from TRIzol extracts of mock-infected and SARS-CoV-infected Vero cells. Blots were probed with polyclonal anti-MHV N antibody (left panel), monoclonal anti-SARS-CoV M antibody (middle panel), or monoclonal anti-MHV M antibody (right panel). (C) Plaques of the MN3 mutant (passage 2 stock) at 33, 37 or 39^{o}C compared with those of isogenic wild-type virus (passage 3 stock). Plaque titrations were carried out on L2 cells; monolayers were stained with neutral red at 72 h postinfection

749 and were photographed 18 h later. Infectious titers measured at all three temperatures were 8.6 x 10^7
750 PFU/ml for wild type and 2.3 x 10^6 PFU/ml for MN3.
751
752 **FIG 3** Effect of E protein mutations on SARS-CoV M chimeras. (A) Alignment of MHV and
753 SARS-CoV E proteins showing independent reverting mutations that enhance the growth of the
754 MN3 chimera at 39°C. The solid bar marks the Tm domain; the circled mutation of MN3rev3 (F20S)
755 was chosen for incorporation into subsequent constructs. GenBank accession numbers for the
756 sequences shown are: MHV-A59, AY700211; and SARS-CoV strain Urbani, AY278741. (B)
757 Schematics of wild-type virus and chimeras containing mutant E, M, and N proteins. Shading
758 represents SARS-CoV sequence substituted for that of MHV. (C) Plaques of wild-type, MN3,
759 MN3rev3, MN6, and MN7 viruses at 37 and 39°C (passage 4 stock for wild type, passage 2 stocks
760 for mutants). Plaque titrations were carried out on L2 cells; monolayers were stained with neutral red
761 at 72 h postinfection and were photographed 18 h later. Measured infectious titers (PFU/ml) at each
762 temperature are indicated.
763
764 **FIG 4** Intramolecular M protein chimeric substitutions. (A) Schematics of wild-type virus and
765 chimeras MN8, MN9, and MN10 containing mutant E, M, and N proteins. Shading represents
766 SARS-CoV sequence substituted for that of MHV. (B) Plaques of wild-type, MN8, MN9, and MN10
767 viruses at 37°C (passage 4 stock for wild type, passage 3 stocks for mutants). Plaque titrations were
768 carried out on L2 cells; monolayers were stained with neutral red at 72 h postinfection and were
769 photographed 18 h later. Measured infectious titers (PFU/ml) are indicated. (C) Schematics of lethal
770 substitutions in chimeras MN4A-C and MN5A-B made in attempts to define a carboxy-terminal
771 subregion of the M endodomain sufficient for interaction with domain N3. MN5A and MN5B also
772 contained the MHV E gene mutation F20S.

773 **FIG 5** Analysis of MN8 mutant virions. MN8 and wild-type virions were purified by equilibrium
774 centrifugation on continuous gradients of 20 to 30% iodixanol that were collected in 15 fractions, as
775 detailed in Materials and Methods. (A) Infectious titers determined for viral peak fractions 4 through
776 11 for MN8 (shaded bars) and wild type (open bars). Densities of all fractions were measured by
777 refractometry (triangles, MN8; circles, wild type). (B, C) Western blots of virion proteins in each
778 fraction probed with polyclonal anti-N (MHV) and monoclonal anti-M-ectodomain (MHV)
779 antibodies. (D, E) Northern dot blots of serial 2-fold dilutions of purified virion RNA detected with a
780 probe specific for genomic RNA. (F) Total protein, genomic RNA (gRNA), and infectivity for wild-
781 type and MN8 virions. Chemiluminescence was quantitated for N protein, M protein, and gRNA,
782 and summed over fractions 3 through 12; values are expressed relative to wild type. Total infectivity
783 (PFU) was summed over fractions 4 through 11.
784
785 **FIG 6** Deficiency of S protein in MN8 virions. (A) Viral peak fractions from iodixanol gradients
786 (fractions 7-10 for wild type and 4-7 for MN8) were separated in 12% SDS-PAGE and analyzed by
787 Western blot probed with a polyclonal antibody specific for the carboxy terminus of S protein, as
788 well as with polyclonal anti-N and monoclonal anti-M antibodies. At the right is a longer exposure
789 of MN8 fraction 5 to allow visualization of S. (B) Western blot of lysates from mouse 17Cl1 cells
790 infected with wild-type or MN8 virus, separated in 8% SDS-PAGE, probed with polyclonal anti-S
791 antibody; *mock*, uninfected 17Cl1 cells. (C) Western blot of wild-type and MN8 virions separated in
792 15% SDS-PAGE and probed with polyclonal anti-S antibody. (D) Western blot of purified wild-
793 type, MN8, MN3, and MN3rev3 virions separated in 8% SDS-PAGE and probed with polyclonal
794 anti-S antibody. (A-D) S_0, 180-kDa uncleaved S protein; S_2, 90-kDa carboxy-terminal cleavage
795 product of S; S_C, carboxy-terminal fragment of S. (E) Schematic of lethal substitution in chimera
796 MN11, which did not rescue the S protein deficiency in MN8.

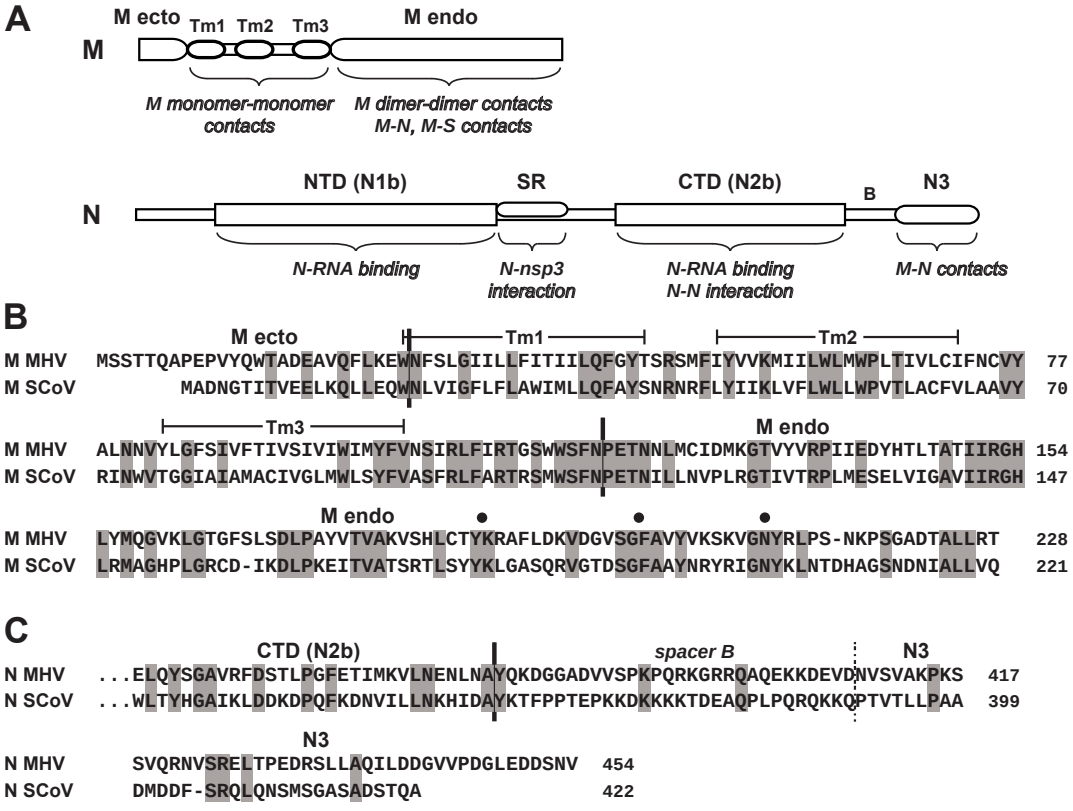

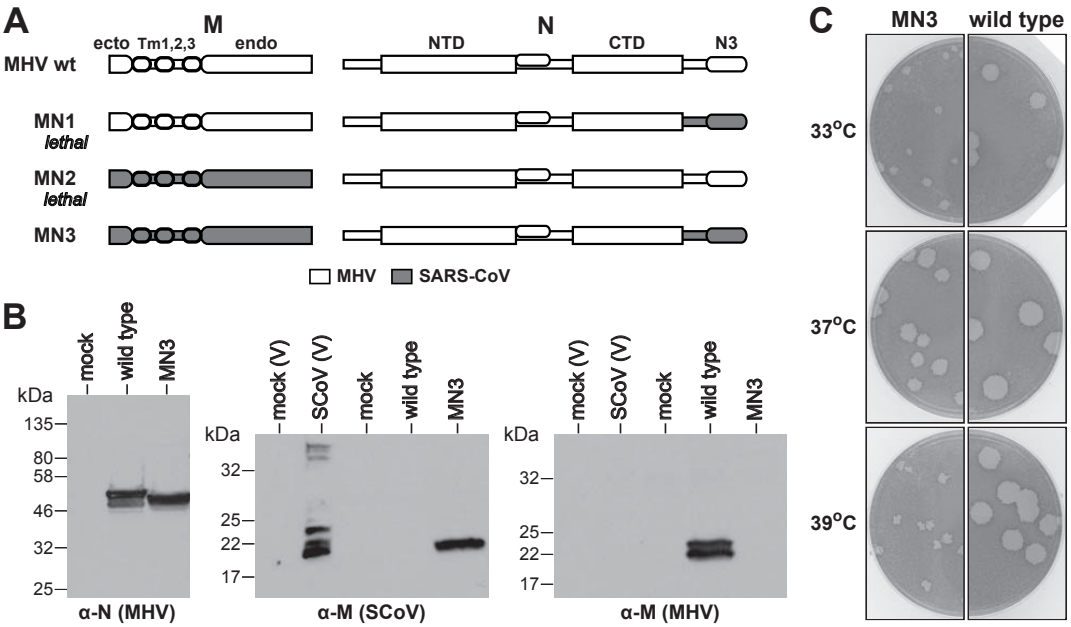

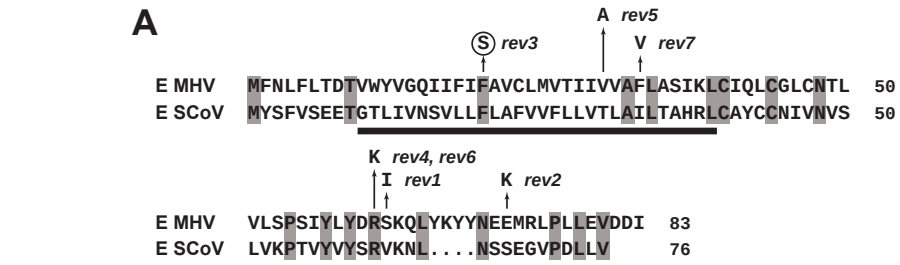

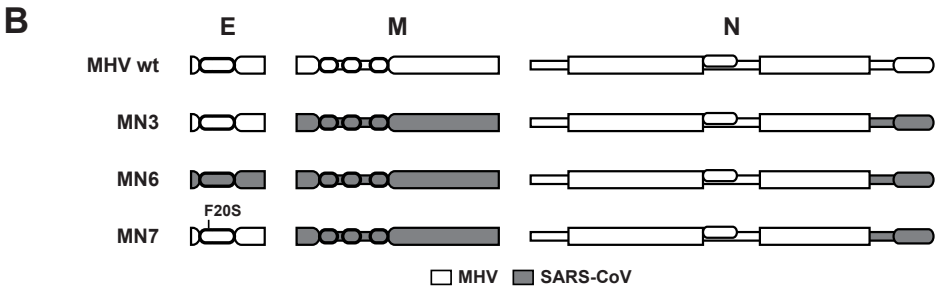

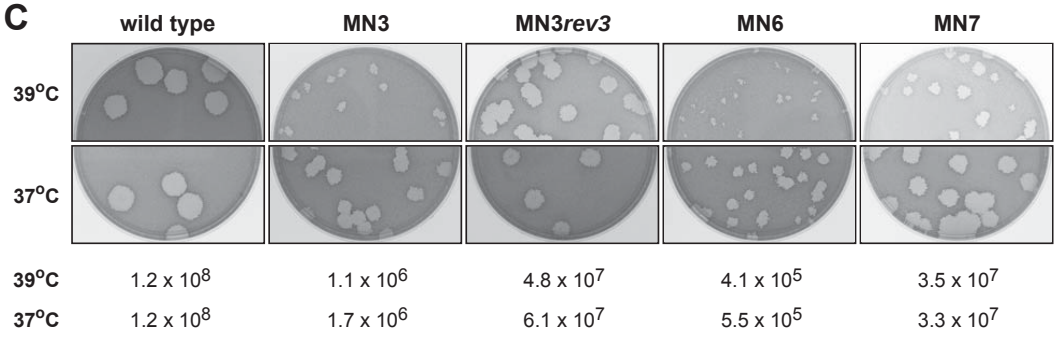

	wild type	MN3	MN3*rev3*	MN6	MN7
39°C	1.2×10^8	1.1×10^6	4.8×10^7	4.1×10^5	3.5×10^7
37°C	1.2×10^8	1.7×10^6	6.1×10^7	5.5×10^5	3.3×10^7

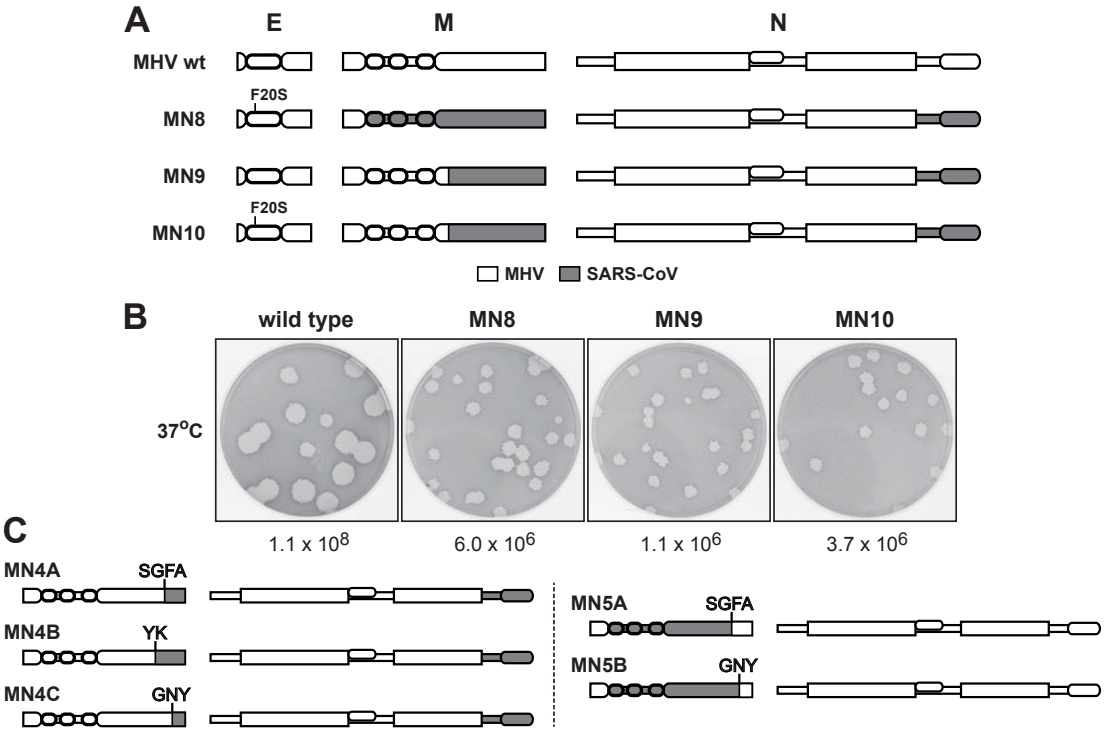

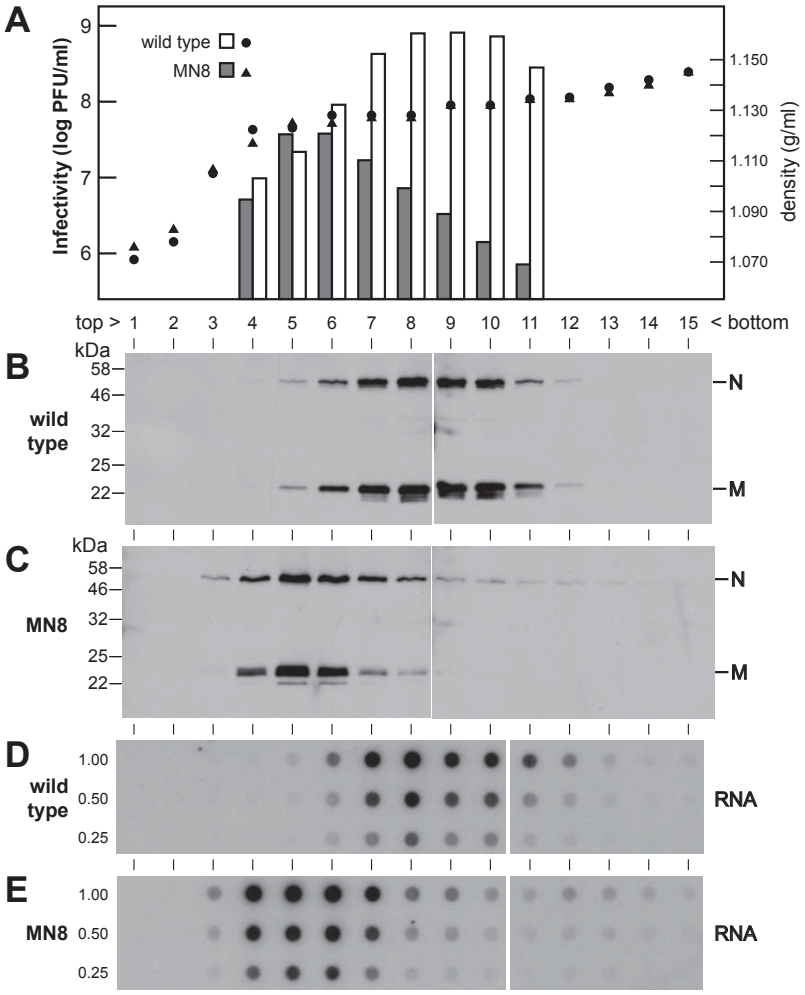

F

	N protein	M protein	gRNA	PFU
wild type	1.00	1.00	1.00	3.56×10^{10}
MN8	1.05	0.85	1.58	1.23×10^{9}